ANS MC2015 - Joint International Conference Mathematics and Computation (M&C), Super Computing in Nuclear Applications (SNA) and the Monte Carlo (MC) Method • Nashville, TN • April 19-23, 2015, on CD-ROM, American Nuclear Society, LaGrange Park, IL (2015)

A HIGH-ORDER LOW-ORDER ALGORITHM WITH EXPONENTIALLY-CONVERGENT MONTE CARLO FOR THERMAL RADIATIVE TRANSFER

Simon R. Bolding and Jim E. Morel
Department of Nuclear Engineering
Texas A&M University
College Station, TX 77843
sbolding@tamu.edu; morel@tamu.edu

Mathew A. Cleveland
Los Alamos National Laboratory
Los Alamos, NM 87545
cleveland@lanl.gov

ABSTRACT

We have implemented a new high-order low-order (HOLO) algorithm for solving thermal radiative transfer (TRT) problems. The low-order (LO) system is based on spatial and angular moments of the transport equation and a linear discontinuous finite-element spatial representation, producing equations similar to the standard S_2 equations. The LO solver is fully implicit in time and efficiently resolves the non-linear temperature dependence at each time step. The HO solver utilizes exponentially-convergent Monte Carlo (ECMC) to give a globally accurate solution for the angular intensity to a fixed-source, pure absorber transport problem. This global solution is used to compute consistency terms that require the HO and LO solutions to converge to the same solution. The use of ECMC allows for efficient reduction of statistical noise in the MC solution, eliminating inaccuracies introduced through the LO consistency terms. We compare results with an implicit Monte Carlo (IMC) code for one-dimensional gray test problems and demonstrate the efficiency of ECMC over SMC in this algorithm.

Did not define SMC

Key Words: hybrid Monte Carlo, residual Monte Carlo, thermal radiative transfer, high order low order

1. INTRODUCTION

We have implemented a high-order low-order (HOLO) algorithm for the case of gray, one spatial dimension TRT problems. The governing equations are the radiation and material energy balance equations, i.e.,

Why not use phi?

$$\frac{1}{c}\frac{\partial I}{\partial t} + \mu\frac{\partial I}{\partial x} + \sigma_t I = \frac{\sigma_s}{2}\phi + \frac{1}{2}\sigma_a acT^4 \quad (1)$$

$$\rho c_v \frac{\partial T}{\partial t} = \int_{-1}^{1} \sigma_a I(x,\mu)\mathrm{d}\mu - \sigma_a ac(T^4), \quad (2)$$

Why parentheses?

In the above equations x is the position, t is the time, μ is the x-direction cosine of the angular intensity $I(x,\mu,t)$, and a, c, ρ, and c_v are the radiation constant, speed of light, mass density, and specific heat; σ_a, σ_s, and σ_t are the absorption, scattering, and total opacities (cm^{-1}), respectively. The desired fundamental unknowns are the material temperature $T(x,t)$ and the scalar radiation intensity $\phi(x,t) = \int_{-1}^{1} I(x,\mu,t)\mathrm{d}\mu$. The equations are strongly coupled through the gray Planckian emission source $\sigma_a acT^4$, which is a nonlinear function of temperature, and the absorption term $\sigma_a\phi$. In general, the material properties are a function of T, introducing additional non-linearity. The non-linear material properties and absorption-reemission physics lead to systems that require solution in a mix of streaming and optically-thick, diffusive regions.

temperature from the transport equation.

Monte Carlo (MC) solution to the TRT equations is typically achieved by the implicit Monte Carlo (IMC) method, first introduced by Fleck and Cummings [1]. This method linearizes the emission source in time to eliminate the material energy equation from the system. The remaining transport equation contains an approximate emission source, as well as an effective scattering cross section representing absorption and reemission over a time step. In optically thick regions, or for large time steps, the effective scattering dominates interactions. In these diffusive regions IMC becomes computationally expensive. Additionally, the approximate linearization of the emission source is not iterated on within a time step, limiting the time step size to produce physically accurate results.

Moment-based hybrid Monte Carlo (MC) methods provide an alternative solution method. Recent work has focused on fixed-point iteration high-order low-order (HOLO) approaches [2–5]. Such methods utilize a low-order (LO) operator based on angular moments of the transport equation, formulated over a coarse spatial mesh. Physics operators that are time consuming for MC to resolve, e.g., absorption-reemission and scattering events, are moved to the LO system. Newton methods allow for non-linearities in the LO equations to be fully resolved efficiently [2]. The high-order (HO) system is defined by Eq. (1), with sources estimated from the LO solution that are truly implicit in time. The HO system is solved via MC to produce a high-fidelity solution for the angular intensity. The MC estimate of the angular intensity is used to estimate consistency terms, present in the LO equations, that require the LO system to preserve the angular accuracy of the MC solution; the HO system does not directly estimate a new material temperature, eliminating stability issues that require linearization of the emission source. However, sufficient MC histories must be performed to eliminate statistical noise in the consistency terms, which can contaminate the LO solution.

and less cpu time per history

In this work, we demonstrate the utility of an S_2-like LO operator in conjunction with an exponentially-convergent Monte Carlo (ECMC) method [6] for the HO solver. The ECMC algorithm allows for statistical noise to be reduced to the same order as the HOLO iteration error with significantly less particle histories than standard MC simulations. We have derived the LO operator directly from the transport equation, using a linear-discontinuous (LD) finite-element (FE) spatial discretization, such that the HO and LO solutions are consistent upon convergence. Herein we describe the algorithm and present results for two test problems.

1.1. Overview of the HOLO Algorithm

For simplicity, our HOLO method will use a backwards Euler discretization in time, as well as constant specific heats and cell-wise constant opacities. The time discretized equations are

$$\mu\frac{\partial I^{n+1}}{\partial x}+\left(\sigma_t+\frac{1}{c\Delta t}\right)I^{n+1}=\frac{\sigma_s}{2}\phi^{n+1}+\frac{1}{2}\left(\sigma_a acT^4\right)^{n+1}+\frac{I^n}{\Delta tc} \tag{3}$$

$$\rho c_v\frac{T^{n+1}-T^n}{\Delta t}=\sigma_a\phi^{n+1}-\sigma_a ac(T^4)^{n+1}. \tag{4}$$

where Δt is the time step size and the superscript n is used to indicate the n-th time step. The algorithm is formed such that the HO and LO solvers can be iterated between until convergence.

In the HOLO context, the LO solver models the physical scattering and resolves the material temperature spatial distribution $T(x)$ at each time step. The LO equations are formed via half-range angular and spatial moments of Eq. (3) and Eq. (4), formed over a spatial finite element mesh. The LO equations take the same form as those used in the hybrid-S_2 method in [7], with element-averaged consistency parameters that are analogous to a variable Eddington factor. If the angular consistency parameters were estimated exactly, then the LO equations are exact with respect to the chosen spatial discretization. These consistency

parameters are lagged in each LO solve, estimated from the previous HO solution for $I^{n+1}(x,\mu)$, as explained below. For the initial LO solve within a time step, the parameters are calculated based on the $I^n(x,\mu)$. The LO equations always conserve energy, independent of the accuracy of the consistency terms.

The solution to the LO system is used to construct a spatially LD representation of the scattering and emission sources on the right hand side of Eq. (3). This defines a fixed-source, pure absorber transport problem for the HO operator. This HO transport problem represents a characteristic method that uses MC to invert the continuous streaming plus removal operator with an LD representation of sources. We will solve this transport problem using ECMC. The output from ECMC is $\tilde{I}(x,\mu)$, a space-angle LD FE projection of the exact solution for $I(x,\mu)$. This projection has minimal statistical noise due to the residual formulation used by the ECMC algorithm. Once computed, $\tilde{I}(x,\mu)$ is used to directly evaluate the necessary LO consistency parameters for the next LO solve. Since there is a global, functional representation of the angular intensity, LO parameters are estimated using quadrature and do not require additional tallies. The HO solution is not used to directly estimate a new temperature at the end of the time step; it is only used to estimate the angular parameters in the LO solution, which eliminates typical operator splitting stability issues that require linearization of the emission source.

One HOLO fixed-point iteration k denotes the process of an ECMC solve of the HO problem to estimate LO parameters, based on the current LO estimate of sources, followed by a solution of the LO system for $T^{n+1}(x)$ and $\phi^{n+1}(x)$. The outer HOLO iterations can be performed until successive LO estimates of $\phi^{n+1}(x)$ and $T^n(x)$ are converged to a desired precision, within each time step. The consistency terms force the HO and LO solutions for $\phi^{n+1}(x)$ to be consistent to the order of the current HOLO iteration error. The HOLO algorithm, for the n-th time step, is

1. Perform a LO solve to produce an initial guess for $T^{n+1,0}(x)$ and $\phi^{n+1,0}(x)$, based on consistency terms estimated with $\tilde{I}^n$.
2. Solve the HO system for $\tilde{I}^{n+1,k+1/2}(x,\mu)$ using ECMC, based on the current LO estimate of the emission and scattering sources.
3. Compute LO consistency parameters with $\tilde{I}^{n+1,k+1/2}$.
4. Solve the LO system using HO consistency parameters to produce a new estimate of $\phi^{n+1,k+1}$ and $T^{n+1,k+1}$ at t_{n+1}.
5. Repeat 2 – 4 until convergence is achieved.
6. Move to the next time step.

where the superscript k denotes an outer HOLO iteration.

2. Forming the Low-Order System

To form the LO system of equations, spatial moments are taken over each spatial cell i: $x \in [x_{i-1/2}, x_{i+1/2}]$, weighted with the standard linear FE interpolatory basis functions. For example, the L moment operator is defined by

$$\langle\cdot\rangle_{L,i} = \frac{2}{h_i}\int_{x_{i-1/2}}^{x_{i+1/2}} b_L(x)(\cdot)\mathrm{d}x, \tag{5}$$

where $h_i = x_{i+1/2} - x_{i-1/2}$ is the width of the spatial element and $b_L(x) = (x_{i+1/2} - x)/h_i$ is the FE basis function corresponding to position $x_{i-1/2}$. The right moment $\langle\cdot\rangle_R$ is defined with weight function $b_R(x) = (x - x_{i-1/2})/h_i$. Here, it is noted that $\phi_{L,i}$ and $\phi_{R,i}$ represent the values of the scalar intensity at

$x_{i-1/2}$ and $x_{i+1/2}$ that preserve the zeroth and first moments over the cell, not to be confused with $\langle\phi\rangle_L$ and $\langle\phi\rangle_R$, which represent spatial moments. To reduce the angular dimensionality, positive and negative half-range integrals of the angular intensity are taken. The half-range averages of I are defined as $\phi^+(x) = \int_0^1 I(x,\mu)\mathrm{d}\mu$ and $\phi^-(x) = \int_{-1}^0 I(x,\mu)\mathrm{d}\mu$, respectively. Thus, in terms of half-range quantities, $\phi(x) = \phi^-(x) + \phi^+(x)$.

2.1. Radiation ~~Balance~~ Energy Equations

Pairwise application of the L and R basis moments with the $+$ and $-$ half-range integrals to Eq. (3) ultimately yields four radiation ~~balance~~ moment equations per cell. As in [7], algebraic manipulation is performed to form intensity-weighted averages of μ, which we call consistency terms. As an example, the final equation resulting from application of the L moment and positive half-range integral is

$$-2\mu^{n+1,+}_{i-1/2}\phi^{n+1,+}_{i-1/2} + \langle\mu\rangle^{n+1,+}_{L,i}\langle\phi\rangle^{n+1,+}_{L,i} + \langle\mu\rangle^{n+1,+}_{R,i}\langle\phi\rangle^{n+1,+}_{R,i} + \left(\sigma_t^{n+1} + \frac{1}{c\Delta t}\right)h_i\langle\phi\rangle^{n+1,+}_{L,i} - \frac{\sigma_s h_i}{2}\left(\langle\phi\rangle^{n+1,+}_{L,i} + \langle\phi\rangle^{n+1,-}_{L,i}\right) = \frac{h_i}{2}\langle\sigma_a^{n+1}acT^{n+1,4}\rangle_{L,i} + \frac{h_i}{c\Delta t}\langle\phi\rangle^{n,+}_{L,i}, \quad (6)$$

where the $\phi^+_{i-1/2}$ and $\mu^+_{i-1/2}$ terms represent angular averaged quantities on the face at $x_{i-1/2}$. The negative direction and R moment equations are derived analogously. Opacities are assumed constant over each element, evaluated at the average temperature in the element, i.e., $\sigma_a = \sigma_a([T_{L,i} + T_{R,i}]/2)$, $x \in (x_{i-1/2}, x_{i+1/2})$. The angular consistency terms are defined in terms of half-range averages, e.g.,

$$\langle\mu\rangle^+_{L,i} = \frac{\frac{2}{h_i}\int_0^1\int_{x_{i-1/2}}^{x_{i+1/2}}\mu\, b_L(x)I^{n+1}(x,\mu)\mathrm{d}x\mathrm{d}\mu}{\frac{2}{h_i}\int_0^1\int_{x_{i-1/2}}^{x_{i+1/2}} b_L(x)I^{n+1}(x,\mu)\mathrm{d}x\mathrm{d}\mu}. \quad (7)$$

2.2. Material ~~Balance~~ Energy Equations

To derive the LO material energy equations, first $T(x)$ is represented spatially in the LD trial space, i.e., $T(x) \simeq T_{L,i}b_L(x) + T_{R,i}b_R(x), \quad x \in (x_{i-1/2}, x_{i+1/2})$. Similarly, the emission term is represented in the material and radiation equations with the LDFE interpolant of $T^4(x)$. The L and R spatial moments are taken of the material energy equation, using these definitions for $T(x)$ and $\sigma_a acT^4(x)$. For example, the final LO material energy equation resulting from application of the L moment is

$$\frac{\rho c_v}{\Delta t}\left[\left(\frac{2}{3}T_{L,i} + \frac{1}{3}T_{R,i}\right)^{n+1} - \left(\frac{2}{3}T_{L,i} + \frac{1}{3}T_{R,i}\right)^{n}\right] + \sigma_a^{n+1}\left(\langle\phi\rangle^+_{L,i} + \langle\phi\rangle^-_{R,i}\right)^{n+1} = \sigma_a^{n+1}ac\left(\frac{2}{3}T^4_{L,i} + \frac{1}{3}T^4_{R,i}\right)^{n+1}. \quad (8)$$

Because the material energy balance only contains angularly integrated quantities, there is no need to take angular moments of the above equation.

2.3. Closing the System with Information from the HO solution

The six degrees of freedom (DOF) over each cell i are the four moments $\langle\phi\rangle^+_{L,i}$, $\langle\phi\rangle^+_{R,i}$, $\langle\phi\rangle^-_{L,i}$, and $\langle\phi\rangle^-_{R,i}$ and the two spatial LDFE edge values $T_{L,i}$ and $T_{R,i}$. The four radiation and two material energy equations

define a system of equations for the six DOF, coupled to other cells via upwinding in the streaming term. However, the angular consistency parameters (e.g., Eq. (7)) are not known a priori, and there is no relation between the volume and face averaged quantities. A lagged estimate of I^{n+1} from the previous HO solve is used to estimate the angular consistency parameters. In the HOLO context, the equations for LO unknowns at iteration $k+1$ use consistency parameters computed using (via relations, e.g., Eq. (7)) with the latest HO solution $\tilde{I}^{n+1,k+1/2}$ as an approximation for $I^{n+1}(x,\mu)$. To close the LO system spatially, the usual LD upwinding approximation is used. For example, for positive flow (e.g., Eq. (6)) the face terms $\mu_{i-1/2}$ and $\phi_{i-1/2}$ are upwinded from the previous cell $i-1$ or from a boundary condition; the terms at $x_{i+1/2}$ are linearly extrapolated, computed using the L and R basis moments, e.g., $\phi^+_{i+1/2} = 2\langle\phi\rangle^+_R - \langle\phi\rangle^+_L$. Because the HO ECMC solver uses an LD representation, this LO spatial closure is inherently consistent. Because there are no spatial temperature derivatives, there is no evaluation of T at faces and thus no need for an additional closure in T.

The LD closure is not strictly positive. In particular, for optically thick cells with a steep temperature gradient, the solution is driven negative. In thick regions of TRT problems, reasonably fine spatial cells can still be on the order of millions of mean free paths; negativities with a LD representation are unavoidable in practice for such cells and mesh refinement is of minimal use. Typically, for a standard LDFE method, the equations are lumped to produce a strictly positive solution. However, standard FE lumping procedures would introduce difficulties in computing the consistency terms from the HO solution. An alternative ~~discontinuous spatial discretization is used that uses a relation between the spatial moments and outflow that produces the same result as~~ spatial closure is used that is equivalent to the standard FE lumping procedure. The L and R moments are defined the same as before, preserving the same average within a cell, but the relation between the moments and the outflow is modified ~~to force a strictly positive outflow~~. For example, for positive μ, the outflow is now defined as $\phi^+_{i+1/2} = \langle\phi\rangle^+_R$. Because the basis function $b_R(x)$ is strictly positive, the outflow is inherently positive. This closure is only used in cells in which negativities occur.

2.4. Solving the Non-Linear LO System

We have used Newton's method to solve the global system of coupled LO equations, based on a typical linearization of the Planckian source with opacities evaluated at lagged temperatures, as described in [8]. Newton iterations are repeated until $\phi^{n+1}(x)$ and $T^{n+1}(x)$ are converged to a desired relative tolerance. The lumping-equivalent discretization discussed above is used for cells where the solution for ϕ^{n+1} becomes negative. When negativities are detected, the lumping-equivalent discretization is used within those cells and that Newton step is repeated.

3. The ECMC High Order Solver

The transport equation to be solved by the HO solver is

$$\mu\frac{\partial I^{n+1,k+1/2}}{\partial x} + \left(\sigma_t^k + \frac{1}{c\Delta t}\right) I^{n+1,k+1/2} = \frac{\sigma_s^k}{2}\phi^{n+1,k} + \frac{1}{2}\left(\sigma_a^k acT^4\right)^{n+1,k} + \frac{\tilde{I}^n}{c\Delta t} \tag{9}$$

where the superscript k represents the outer HOLO iteration index. Material property indices will be suppressed from now on. Here, $k+1/2$ denotes the ECMC solution within outer HOLO iteration k, whereas k and $k+1$ represent successive LO solves. The sources at k are estimated by the previous LO solution. Opacities are ~~based on~~ evaluated at $T^{n+1,k}$. As all sources on the right side of the equation are known, this defines a fixed-source, pure absorber transport problem. We will solve this equation using ECMC. A more detailed description of the ECMC method can be found in [9], but a brief overview is given here.

In operator notation, the previous equation can be written as

$$\mathbf{L}^k I^{n+1,k+1/2} = q^k \tag{10}$$

where $I^{n+1,k+1/2}$ is the transport solution of the angular intensity based on the k-th LO estimate of q^k. The linear operator $\mathbf{L}^k$ is the streaming plus removal operator defined by the left hand side of Eq. (3). The approximate solution to Eq. (10) (i represents inner HO batches) is represented as $\tilde{I}^{n+1,(i)}$. The i-th residual is defined as $r^{(i)} = q - \mathbf{L}\tilde{I}^{n+1,(i)}$. For reference, the residual at iteration i in the HO solve is

$$r^{(i),k+1/2} = \frac{\sigma_s}{2}\phi_{LD}^{n+1,k} + \frac{1}{2}\left(\sigma_a^* a T^4\right)_{LD}^{n+1,k} + \frac{\tilde{I}^n}{c\Delta t} - \left(\mu\frac{\partial \tilde{I}^{n+1,k+1/2}}{\partial x} + \left(\sigma_t + \frac{1}{c\Delta t}\right)\tilde{I}^{n+1,k+1/2}\right)^{(i)} \quad (11)$$

where the k terms are LD in space on the coarsest mesh and are not recalculated at any point during the HO solve. The functional form of $\tilde{I}^n$ is defined over the finest space-angle mesh from the final HOLO iteration of the previous time step.

To define the ECMC algorithm, the HOLO iteration indices are dropped, as the LO estimated q^k and $\mathbf{L}^k$ remain constant over the entire HO solve. Addition of $\mathbf{L}I^{n+1} - q = 0$ to the residual equation and manipulation of the result yields the error equation

$$\mathbf{L}(I^{n+1} - \tilde{I}^{n+1,(i)}) = \mathbf{L}\tilde{\epsilon}^{(i)} = r^{(i)} \quad (12)$$

where I^{n+1} is the exact solution and $\tilde{\epsilon}^{(i)}$ is finite element representation of the error in $\tilde{I}^{n+1,(i)}$. The above equation is inverted yielding the Monte Carlo estimate of the error in $\tilde{I}^{n+1,(i)}$, i.e.,

$$\tilde{\epsilon}^{(i)} = \mathbf{L}^{-1}r^{(i)} \quad (13)$$

where $\mathbf{L}^{-1}$ is the Monte Carlo inversion of the streaming and removal operator. Here, we emphasize the solution $\tilde{I}^{n+1,(i)}$ represents the projection of the exact Monte Carlo solution onto the trial space. This is in general far more accurate than a standard finite element solution. For example, the LD trial space preserves the zeroth and first spatial moment over a cell; the zeroth moment is computed using a standard path-length volumetric flux tally, which is equivalent to typical volumetric averages computed in Monte Carlo calculations. The primary truncation error is in the LD representation of the right hand side source terms and residual at each iteration. Only volumetric flux tallies over all of the finest space-angle elements are used; tallies are computed for the average, slope in x, and slope in μ of $I^{n+1}(x,\mu)$ by weighting the tallies for I^{n+1} with the appropriate basis function.

The ECMC algorithm is

1. Initialize the guess for $\tilde{I}^{n+1,(0)}$ to $\tilde{I}^n$ or the projection of $\tilde{I}^{n+1}$ from the latest HO solve
2. Compute $r^{(i)}$.
3. Solve $\tilde{\epsilon}^{(i)} = \mathbf{L}^{-1}r^{(i)}$
4. Compute a new estimate of the intensity $\tilde{I}^{n+1,(i+1)} = \tilde{I}^{n+1,(i)} + \tilde{\epsilon}^{(i)}$
5. Repeat steps 2 – 4 until desired convergence criteria is achieved.

The initial guess for the angular intensity $I^{n+1,(0)}$ is computed based on the previous solution for $\tilde{I}^n$. This is a critical step in the algorithm; it significantly reduces the required number of particles per time step because I does not change drastically between time steps in optically thick regions. It is noted that the ECMC batch (steps 1-4 of the algorithm) results in essentially the same estimate of the solution as the residual formulation used in [4]. The primary difference is that our method uses an LD trial space, and we are able to use our new estimate of the solution to recompute a residual.

Exponential convergence is obtained because with each batch a better estimate of the solution is being used to compute the new residual, decreasing the magnitude of the Monte Carlo source each iteration i, relative

to the solution I^{n+1}. Each Monte Carlo estimate of ϵ still has a computable statistical uncertainty. If the statistical estimate of $\tilde{\epsilon}$ is not sufficiently accurate, then the iterations would diverge. Because the exact angular intensity does not in general lie within the LD trial space, the iterative estimate of the error will eventually stagnate once the error cannot be sufficiently represented by a given LDFE mesh. Although mesh refinement is not performed in the calculations presented here ~~this work~~, an adaptive $h-$refinement algorithm has been implemented that can be used to allow the system to continue converging towards the exact solution.

3.1. Variance Reduction and Source Biasing

As in [3], because we are solving a pure absorber problem with Monte Carlo, we will allow particles to stream without absorption to reduce statistical variance in the tallies. The weight of particles is reduced deterministically along the path as they stream, with no need to sample a path length. Because particles are exponentially attenuated, the normalized weight is adjusted as $w(x) = w(x_0)exp(-|(x - x_0)/\mu|)$, where x_0 is the starting location of the path. The tallies are modified to account for the continuously changing weight. Histories are allowed to stream in this manner for 6 mean free paths before switching to analog path length sampling; this prevents the tracking of very small weight histories.

As another way to improve efficiency and statistics, a modified systematic sampling method [10] was used for determining source particle locations. The goal is to effectively distribute particle histories to regions of importance, but to sample a sufficient number of histories in less probable regions to prevent large statistical noise. However, there is no need to sample histories in regions that are in equilibrium and the solution is not changing over a time step. The residual gives a good indication of where particles are most likely to contribute to the error, particularly in optically thick cells. In the sampling algorithm the number of particle histories sampled in each space-angle cell is predetermined and proportional to the magnitude of the residual in that cell. Then, for the predetermined number of histories within a cell, the source location is randomly sampled according to the source distribution within that cell. There is a relative probability cutoff such that cells with an insignificant residual will have no histories sampled there. In these regions the problem is remaining in steady state and the solution is known exactly. For cells that are significant, but have a predetermined number of histories below some preset minimum N_{min}, the number of histories sampled in that cell is set to N_{min}. This is to limit bad statistics in low probability cells, particularly in the case of adaptively refined meshes. In the simulations performed for this work N_{min} is set to one. This is done for comparing to IMC to keep the total number of histories per time step constant throughout the entire simulation.

3.2. Fixup Near the Wave-Front

For the HO solver, in cells near the radiation wave front, the LD trial space results in negativities in $\tilde{I}^{n+1}(x, \mu)$, as with the LO solver. Currently, we do not treat these cells specially and just check the consistency terms at the end of the HO solve and detect if they lie in the appropriate half-space. If the terms are non-physical, then they are set to S_2-equivalent terms. This may lead to artificially fast wave-speeds in certain cells. Future work will include using a different trial space in these cells that is strictly positive.

4. Results

4.1. Marshak Wave

We will compare results of the HOLO method to IMC with a source tilting algorithm [11]. In IMC the material and radiation energy fields are discretized spatially to solve for cell-averaged values. Inaccurate spatial representation of the emission source over a cell can result in energy propagating through the domain artificially fast, yielding non-physical results referred to as “teleportation error”. The IMC method

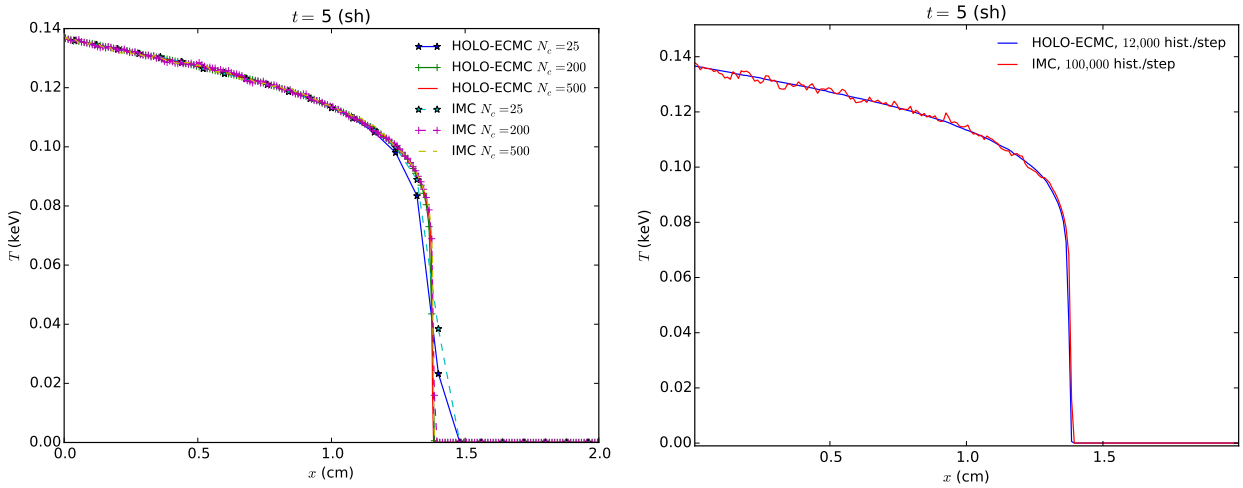

(a) Convergence of IMC and HOLO-ECMC solutions.

(b) Comparison of solutions for 200 spatial cells.

Figure 1: Comparison of solutions for Marshak wave problem at t = 5 sh.

uses a fixup known as source tilting to mitigate this problem. Source tilting reconstructs a more accurate linear-discontinuous representation of the emission source within a cell based on the cell-averaged material temperatures in adjacent cells. This is not necessary in our method because of the LD representation of the emission source.

cm^{-1}

For the first problem, initially the radiation and material energies are in equilibrium at 2.5E-05 keV. An isotropic incident intensity of 0.150 keV is applied at $x = 0$; the incident intensity on the right boundary is 2.5E-05 keV. The material properties are $\rho = 1$ g cm^{-3} and $c_v = 0.013784$ jks/keV-g. The absorption cross section varies as $\sigma(T) = 0.001\ \rho\ T^{-2}$, which introduces a strong non-linearity into the problem. The simulation ~~was~~ ran for 5 sh (1 sh = 10^{-8} s) with a fixed time step size of 0.001 sh. For comparison purposes, we have not used adaptive mesh refinement, only performed one HOLO iteration per time step, and use a fixed 3 HO batches with equal number of histories per batch. A relative tolerance of 1.E-06 in the norm of $\phi(x)$ and $T(x)$ was used for the LO newton solver. Radiation energy distributions are plotted as an equivalent temperature given by $T_r = \sqrt[4]{\phi/(ac)}$. Cell-averaged quantities are plotted. Although scattering physics can be handled by the LO solver in this method [5], we have only considered pure absorber problems here.

Fig. 1a compares the cell-averaged radiation temperatures for the IMC and HOLO method with ECMC, for various number of spatial mesh cells N_c. For the HOLO solver, we have used 4 equal-sized cells in μ. The solutions agree as the mesh is converged. There is similar agreement in the location of the wave front due to the linear shape of the emission source over a cell. The cells at the wave front required use of the lumping-equivalent discretization during the LO solve, resulting in strictly positive solutions.

Fig. 1b compares solutions for the case of 200 cells. For the IMC solution 10^5 histories per time step were simulated; for the HOLO method only $4,000$ histories per batch (12,000 per time step) were simulated. There is significant statistical noise in the IMC solution compared to the HOLO solution. The relatively small number of histories is possible due to the residual formulation and the initial guess of $\tilde{I}^n$ for the first HO solve. Since the transport solve is only determining the change over the time step, the statistical noise in the result is small relative to the magnitude of I^{n+1}. Also, the source bias only places particles where the residual is large. No particles are sampled in the equilibrium region out front of the wave.

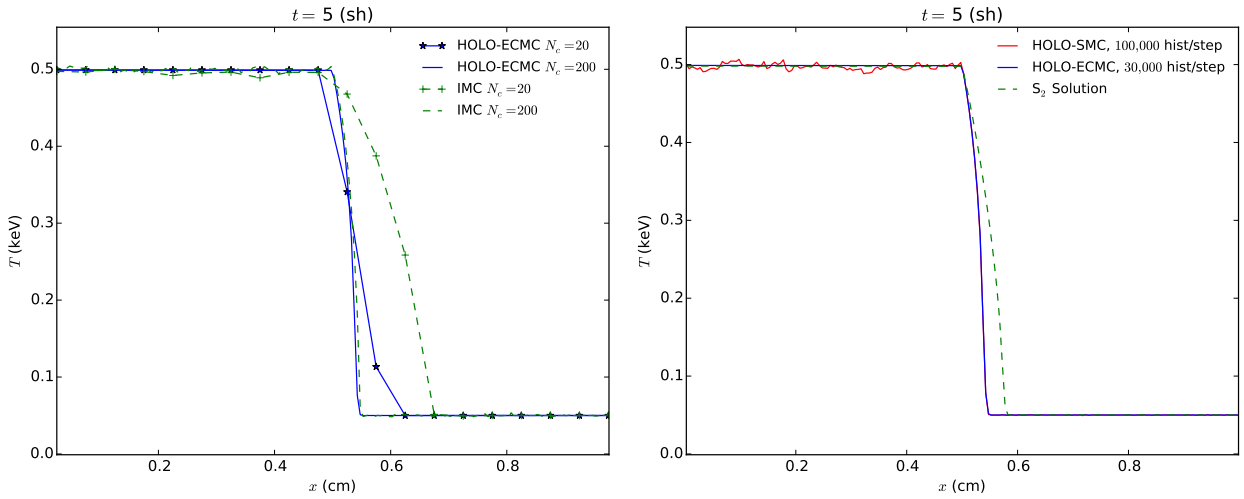

(a) Comparison of IMC and HOLO-ECMC.

(b) Comparison of SMC and ECMC HO solvers.

Figure 2: Comparison of radiation temperatures for two material problem.

4.2. Two Material Problem

This problem consists of an optically thin (left) and an optically thick (right) material region, with constant opacities. The material properties are given in Table I. Initially the radiation and material energies are in equilibrium at a temperature of 0.05 keV. An isotropic incident intensity of 0.500 keV is applied at $x = 0$ at $t = 0$; the isotropic incident intensity on the right boundary is 0.05 keV. The simulation is ran for 5 sh.

Fig. 2b compares the HOLO and IMC radiation temperatures at the end of the simulation. The IMC method used 10^5 histories per time step, where as the HOLO method used 3×10^4 histories per time step. The IMC and HOLO results show good agreement over the finer mesh. On the coarse mesh ($N_c = 20$), the HOLO method predicts the location of the wave-front more accurately than the IMC method.

Fig. **??** compares results for different HO solvers. The HOLO algoirthm with the ECMC HO solver (HOLO-ECMC) results are for running 3 batches of 10,000 histories, per time step. The solution for the HOLO method with a standard MC solver as the HO solver (HOLO-SMC) with standard source sampling uses 10^5 histories per time step. Also plotted, is an S_2 solution obtained by using consistency terms that are equivalent to S$-$2 and no MC correction. The HOLO-SMC solution demonstrates significant statistical noise. This noise is introduced into the LO solver by bad statistics in computing the consistency terms. The S_2 solution results in an artificially fast wave front as expected, demonstrating the necessity of HO correction in this problem.

	$x \in [0, 0.5)$ cm	$x \in [0.5, 1.0]$ cm
σ_a (cm$^-$1)	0.2	2000
ρ (g cm$^-$3)	0.03	10.0
c_v (jks/keV-g)	0.1	0.1

Table I: Two material problem properties

5. Conclusions

We have been able to produce solutions for Marshak ~~Wave~~ wave test problems using a new HOLO method that is in agreement with IMC. Unlike IMC, our method requires no effective scattering events to be included in the MC simulation, limiting the total run time of the simulations; this is also favorable for future parallelization since particles can be allowed to stream to boundaries without interaction. The LD spatial representation mitigates issues with ~~energy propagating through the problem artificially fast,~~ the "teleportation" effect similar ~~in effect~~ to source tilting in the IMC algorithm. The LO solver resolves the non-linearities in the equations resulting in a fully implicit time discretization. The ECMC approach, with initial guesses based on the previous radiation intensity, results in efficient reduction of statistical error and allows for particles to be distributed to largely varying regions of the problem. The LO solver can accurately and efficiently resolve the solution in diffusive regions, while the HO transport solver provides the accuracy of a full transport treatment where necessary.

The primary difficulty to overcome is in the HO solver at the wave front. A strictly positive spatial discretization in the residual formulation needs to be implemented for high accuracy solutions near the wave front. The representation needs to be implemented such that the spatial closure in the LO system is consistent with the HO representation for the solution. The ability to represent the solution accurately in rapidly varying regions of the problem will be key for generalization of this method to higher dimensions. Future work will include comparisons to IMC using a figure of merit that accounts for the fact that our histories consist of pure absorber simulations, which will, in general, be less computationally expensive than IMC. Ultimately, we will apply this method to multi-group TRT equations, before extending to it multiple spatial dimensions.

ACKNOWLEDGEMENTS

This research was performed using funding received from the DOE Office of Nuclear Energy's Nuclear Energy University Programs and under Los Alamos National Security, LLC, for the National Nuclear Security Administration of the U.S. Department of Energy under contract DE-AC52-06NA25396.

REFERENCES

[1] J. A. Fleck, Jr. and J. D. Cummings, Jr., "An Implicit Monte Carlo Scheme for Calculating Time and Frequency Dependent Nonlinear Radiation Transport," *J. Comput. Phys.*, **8**, 3, pp. 313–342 (Dec. 1971).

[2] J. Willert, C. Kelly, D. Knoll, and H. Park, "A Hybrid Approach to the Neutron Transport k-Eigenvalue Problem using NDA-based Algorithms," (2013), M&C.

[3] H. Park, J. Densmore, A. Wollaber, D. Knoll, and R. Ramenzahn, "Monte Carlo Solution Methods in a Moment-Based Scale-Bridging Algorithm For Thermal Radiative Transfer Problems," M&C (2013).

[4] J. Willert and H. Park, "Residual Monte Carlo High-order Solver for Moment-Based Accelerated Thermal Radiative Transfer Equations," *Journal of Computational Physics*, **276**, pp. 405 – 421 (2014).

[5] S. Bolding and J. Morel, "A High-Order Low-Order Algorithm with Exponentially-Convergent Monte Carlo for k-Eigenvalue problems," ANS Winter Meeting (2014).

[6] J. Peterson, J. Morel, and J. Ragusa, "Exponentially Convergent Monte Carlo for the 1-D Transport Equation," M&C (2013).

[7] E. Wolters, *Hybrid Monte Carlo - Deterministic Neutron Transport Methods Using Nonlinear Functionals*, Ph.D. dissertation, Michigan (2011).

[8] J. Morel, T. Wareing, and K. Smith, "Linear-Discontinuous Spatial Differencing Scheme for S_n Radiative Transfer Calculations," *Journal of Computational Physics*, **128**, pp. 445–462 (1996).

[9] J. Peterson, *Exponentially Convergent Monte Carlo for the 1-D Transport Equation*, Master's thesis, Texas A&M (2014).

[10] J. Shultis and W. Dunn, *Exploring Monte Carlo Methods*, Academic Press, Burlington, MA 01803 (2012).

[11] T. Urbatsch and T. Evans, "Milagro Version 2 An Implicit Monte Carlo Code for Thermal Radiative Transfer: Capabilities, Development, and Usage," Los Alamos National Laboratory Report LA-14195-MS (2006).